Journal of Power Sources 210 (2012) 392–396

Contents lists available at SciVerse ScienceDirect

Journal of Power Sources

journal homepage: www.elsevier.com/locate/jpowsour

Short communication

Enhanced electroactivity of Pd nanocrystals supported on $H_3PMo_{12}O_{40}$/carbon for formic acid electrooxidation

Xiao Zhao [a,b], Jianbing Zhu [a,b], Liang Liang [a,c], Changpeng Liu [c], Jianhui Liao [a,c], Wei Xing [a,c,*]

[a] State Key Laboratory of Electroanalytical Chemistry, Changchun Institute of Applied Chemistry, Chinese Academy of Sciences, Changchun, Jilin 130022, China
[b] Graduate School of the Chinese Academy of Sciences, Beijing 100039, China
[c] Laboratory of Advanced Power Sources, Changchun Institute of Applied Chemistry, 5625 Renmin Street, Changchun 130022, China

ARTICLE INFO

Article history:
Received 4 November 2011
Received in revised form 8 January 2012
Accepted 12 January 2012
Available online 21 January 2012

Keywords:
Pd
Polyoxometalates
Pd oxide
Metal–support interaction
Formic acid electrooxidation

ABSTRACT

The preparation of highly dispersed precious metal catalysts is an important subject for fuel cell applications. Here, using a phosphomolybdic acid (PMo_{12})-assisted method, a Pd-PMo_{12}/C catalyst with uniform Pd nanoparticles is prepared. The TEM results show that the presence of PMo_{12} facilitates the formation of uniform Pd particles with an average particle size of 3.2 nm. More importantly, the Pd-PMo_{12}/C catalyst displays an enhanced activity and stability for formic acid electro-oxidation and a better tolerance toward CO poisoning than Pd nanocatalysts prepared with sodium citrate as a stabilizer. A combination of the composition and structure analyses show that the reasons for the improved electro-catalytic activity of the Pd-PMo_{12}/C catalyst involve the metal–support interaction, the richer Pd oxide/hydrous oxide content and the inherent properties of PMo_{12}.

1. Introduction

Recently, formic acid has arisen as an interesting fuel for use in fuel cell technology and has attracted intensive attention due to several attractive features, such as reduced toxicity, higher kinetic activity and lower fuel crossover through Nafion membranes than methanol [1–3]. For anode catalysts applied in direct formic acid fuel cells (DFAFCs), Pd-based materials have been extensively studied because of their higher catalytic activity for the formic acid electro-oxidation reaction (FAEO), lower cost and greater abundance than Pt [4–6]. However, recent progress has shown that a gradually build-up of adsorbed CO (CO_{ads}) or a 'CO-like' intermediate has caused the deactivation of Pd catalysts. As a result, Pd-based DFAFCs possessed a limited lifetime and required a periodic oxidative removal of these poisoning species to restore the full operating power, which has seriously restricted their practical application [7,8]. The poor stability of catalysts is generally caused by irrecoverable/irreversible loss (i.e., the loss of electrochemical surface area due to particle growth/sintering or dissolution, carbon corrosion, etc.) and recoverable/reversible loss (i.e., the accumulation of a poisoning intermediate or other recoverable material changes). Here, the accumulation of poisoning species on the surface of Pd catalysts accelerated their decay rate, and simultaneously, the oxidative treatment to remove the poisoning species sped the dissolution of Pd nano-particles (NPs). This led to the irreversible loss of electrochemical surface area and deteriorated the stability of the Pd catalyst. Therefore, improving the resistance of the Pd catalyst to the poisoning species is a preferable method for alleviating the deactivation of the Pd catalyst compared with the oxidative treatment [7,9–11].

On the other hand, in developing Pd-based anode catalysts, it is important to prepare highly dispersed and stabilized Pd NPs. Generally, the interactions between support and catalytic metals have an important influence on the particle nucleation and growth processes that determine the metal particle size and dispersion. Introducing appropriate functional groups on the support surface is an effective method for facilitating the deposition and dispersion of metal NPs [12,13]. For example, the chemical oxidation treatment of carbon materials (e.g., refluxing in HNO_3 or H_2SO_4/HNO_3 solution) is usually adopted to produce oxygen-containing groups acting as anchor sites (—COOH, —C=O, etc.) [13–15]. Unfortunately, the chemical oxidation method simultaneously introduces structural defects that reduce the electrical conductivity and the durability of the carbon support [14,16]. The effective dispersal of metal NPs onto un-oxidized and complete-structure carbon materials remains an interesting issue. Keggin-type heteropolyacids (HPAs) are known to adsorb irreversibly on carbon and metal surfaces [15,17]. For example, heteropolyanion monolayer-coated electrodes can be formed by simply soaking the electrode in an

* Corresponding author at: Renmin Street, Changchun 130022, China. Tel.: +86 431 85262223; fax: +86 431 85685653.
E-mail address: xingwei@ciac.jl.cn (W. Xing).

0378-7753/$ – see front matter © 2012 Elsevier B.V. All rights reserved.
doi:10.1016/j.jpowsour.2012.01.078

acidic aqueous solution of heteropolyanion [18]. Further, it has been reported that HPAs can enhance the electrocatalytic activity of Pt catalysts for methanol oxidation and oxygen reduction due to their excellent redox properties and high protonic conductivity [15,17,19,20].

In this study, phosphomolybdic acid (PMo_{12}), a keggin-type polyoxometalate, was used to synthesize Pd NPs. Using this method, it was easy to obtain uniform and small-sized Pd NPs (3.2 nm). More importantly, the Pd catalyst prepared by the PMo_{12}-assisted method (Pd-PMo_{12}/C) showed an enhanced activity for the FAEO and a higher tolerance toward CO poisoning than the Pd catalyst prepared with sodium citrate as a stabilizer (Pd/C-citrate).

2. Experimental

2.1. Catalysts preparation

The Pd-PMo_{12}/C catalyst was prepared as follows: 50 mg of Vulcan XC-72 carbon, 215 mg of PMo_{12} and 20.8 mg of $PdCl_2$ (dissolved in 1 M hydrochloric acid) were added to 100 mL of deionized water. The above suspension was ultrasonically dispersed and then stirred for 10 h to ensure that PMo_{12} was adsorbed onto the Vulcan XC 72 carbon. Subsequently, the pH value of the suspension was adjusted to ca. 4.0 with a 50% (V/V) aqueous ammonia solution. Subsequently, 50 mL of a freshly prepared aqueous solution of $NaBH_4$ (44 mg) were added dropwise to deposit the Pd NPs. The mixture was filtered, and the solid was washed with warm deionized water and then dried in a vacuum oven at 80 °C overnight. For comparison, sodium citrate was also used as a stabilizer to prepare the Pd/C catalyst. This synthesis method was similar to the above procedure except that 215 mg of PMo_{12} was replaced by 173 mg of sodium citrate as a stabilizer. The carbon-supported PMo_{12} (PMo_{12}/C) was prepared as follows: 500 mg of Vulcan XC 72 carbon was added to 50 mL of 5 mg mL^{-1} PMo_{12} aqueous solution containing 1 M hydrochloric acid. The suspension was ultrasonically dispersed and then stirred for 10 h. The suspension was filtered, and the solid was washed with warm deionized water and then dried in the vacuum oven at 80 °C overnight.

2.2. Physical characterizations

The size and morphology of the catalysts were analyzed by transmission electron microscopy (TEM) operating at 200 kV (Philips TECNAI G2). The X-ray diffraction (XRD) patterns of the catalysts were obtained using a PW1700 diffractometer (Philips Co.) with a Cu Kα (λ = 0.15405 nm) radiation source operating at 40 kV and 30 Ma. X-ray photoelectron spectroscopy (XPS) was conducted using an ESCALAB MKII photoelectron spectrometer (VG Scientific). The XPS experiments were performed in a spectroscopy chamber using a standard Al anode X-ray source. The Pd 3d and Mo 3d signals were collected and analyzed with deconvolution of the spectra using XPS Peak software. The bulk composition of the catalysts was evaluated by energy dispersive X-ray analysis (EDX) on a JEOL JAX-840 scanning electron microscope operating at 20 kV.

2.3. Electrochemical measurements

All the electrochemical measurements were performed with an EG&G mode 273 potentiostat/galvanostat and a conventional three-electrode test cell at ambient temperature. The catalyst ink was prepared by ultrasonically dispersing the mixture of 5 mg of the catalyst, 950 μL of ethanol, and 50 μL of Nafion alcohol solutions (Aldrich, 5 w/o Nafion). Next, 5 μL of the catalyst ink was pipetted and spread on the 3-mm diameter pre-cleaned glassy carbon disk for use as the working electrode. A Pt foil and a KCl-saturated silver–silver chloride electrode (Ag/AgCl) were used as the counter and reference electrodes, respectively. To evaluate the catalytic activity for the FAEO, the cyclic voltammetry experiments were then performed in 0.5 M H_2SO_4 + 0.5 M HCOOH solution with a scan rate of 20 mV s^{-1}. The chronoamperometric experiments were performed in the same solution at a potential of 0.2 V for 3600 s. The electrochemical surface areas (ESA) of the catalysts were estimated by the CO_{ad} stripping test, assuming that the coulombic charge required for the oxidation of the CO_{ad} monolayer was 420 μC cm^{-2}. All the electrolyte solutions were deaerated by high-purity nitrogen for at least 10 min prior to any measurements.

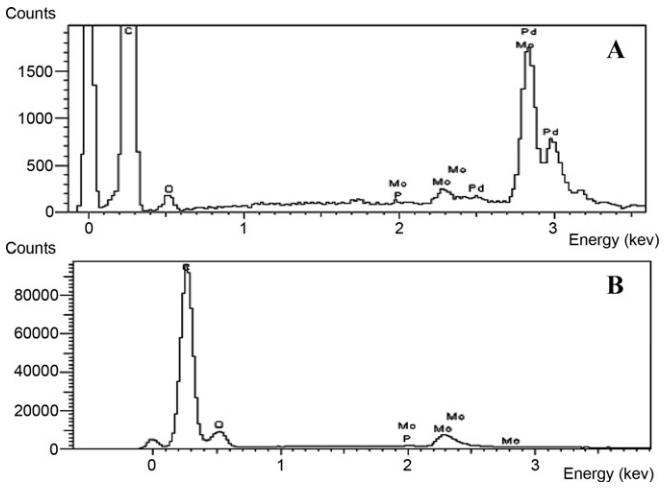

Fig. 1. EDX spectra of the PMo_{12}/C (A) and Pd-PMo_{12}/C catalysts (B).

3. Results and discussion

3.1. EDX, XRD, TEM and XPS analyses

The physical properties of the catalysts were characterized by EDX, XRD, XPS and TEM. EDX was used to detect the presence of PMo_{12} in the carbon support. Fig. 1 shows the EDX spectrum of PMo_{12}/C and the Pd-PMo_{12}/C catalyst. The co-existence of Mo and P characteristic peaks in PMo_{12}/C and the Pd-PMo_{12}/C catalyst reveals that PMo_{12} are adsorbed on the carbon and/or metal surface. The crystalline structures of the catalysts were investigated by XRD analysis. As shown in Fig. 2a, PMo_{12}/C exhibits the characteristic peaks of the C (0 0 2) and (1 0 0) planes at approximately 20° and 25°, respectively. When compared with PMo_{12} (Fig. 2b), PMo_{12}/C shows no noticeable diffraction peaks that can be assigned to crystallized PMo_{12} or Mo oxides. Thus, it could be said that PMo_{12} adsorbed on a carbon surface is in a highly dispersed manner with no agglomeration, which is consistent with previous reports [19,21]. Fig. 2c and d display similar profiles for Pd/C-citrate and Pd-PMo_{12}/C catalysts in which the characteristic peaks of a crystalline face-centered cubic Pd phase can be observed. Similar to PMo_{12}/C, there are no obvious signals for PMo_{12} in the XRD pattern of the Pd-PMo_{12}/C catalyst.

Fig. 3 displays the TEM images and the corresponding size distribution histograms of the Pd-PMo_{12}/C and Pd/C-citrate catalysts. The size distributions were obtained by measuring the sizes of 100 randomly selected particles in the magnified TEM images. As shown in Fig. 3A and B, Pd NPs on the PMo_{12}/C support are remarkably uniform and have a rather narrow size distribution with an average particle size of ca. 3.2 nm. In contrast, the Pd NPs of the Pd/C-citrate catalyst are dispersed in a relatively wide size distribution, and the average particle size is approximately 3.5 nm. This result indicates that the introduction of PMo_{12} for Pd-PMo_{12}/C catalyst is beneficial to the dispersion and stabilization of Pd NPs [15,19,22,23].

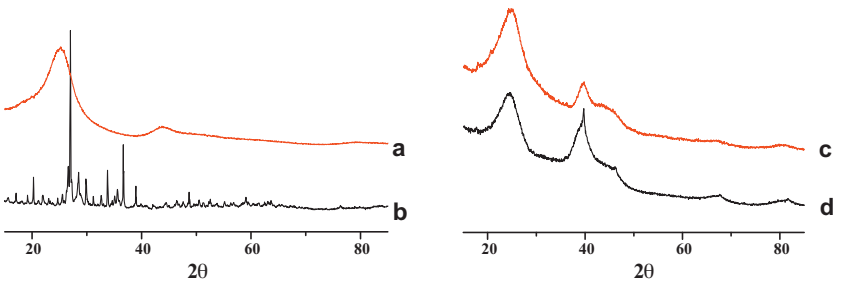

Fig. 2. XRD patterns of PMo_{12}/C (a), PMo_{12} (b), the Pd/C-citrate catalyst (c) and the Pd-PMo_{12}/C catalyst (d).

Specifically, the PMo_{12} adsorbed on the carbon surface offered a large number of uniformly distributed active sites for anchoring Pd NPs [15]. Meanwhile, electrostatic repulsive interactions induced by PMo_{12} anions prevented Pd NPs from agglomerating [19,22].

XPS was used to determine the surface composition of the catalysts and possible electronic interactions. As shown in Fig. 4, the Pd $3d_{5/2}$ signals of the catalysts were deconvolved into three components assigned to metallic Pd, Pd (II) and Pd (IV) species. The binding energies (BE) of the Pd, Pd (II) and Pd (IV) species for the Pd/C-citrate catalyst are ca. 335.50, 336.70, and 337.85 eV, respectively, while those for the Pd-PMo_{12}/C catalyst are ca. 335.70, 336.75, and 338.20 eV, respectively. Clearly, the BE of Pd $3d_{5/2}$ for the Pd-PMo_{12}/C catalyst was shifted to a higher BE direction compared with the Pd/C-citrate catalyst. In addition, the Pd-PMo_{12}/C catalyst displayed a much higher Pd oxide content containing Pd (II) and Pd (IV) species (70%) than the Pd/C-citrate catalyst (52%). Considering a similar particle size between the Pd-PMo_{12}/C and Pd/C-citrate catalysts, the particle size effect should not be responsible for this BE shift and the increased Pd oxide content [24]. It is likely that the metal–support interaction between Pd and PMo_{12}/C accounted for these observations [25]. This type of metal–support interaction can be supported by the analysis of the Mo 3d spectra. Fig. 5A shows the Mo 3d signal of PMo_{12}/C in which the BE of $3d_{5/2}$ and $3d_{3/2}$ are 232.01 and 235.16 eV, respectively, and were assigned to Mo (VI) of PMo_{12} [23]. In contrast, according to Fig. 5B, the BE of $3d_{5/2}$ and $3d_{3/2}$ of Mo (VI) for the Pd-PMo_{12}/C catalyst were ca. 231.92 eV and 235.14 eV, respectively, which shows a negative shift in BE compared with Mo_{12}/C. The BE at ca. 230.9 eV and 234.1 eV can be attributed to the Mo (IV) species, as a result of the reduction of the Mo (VI) species by $NaBH_4$.

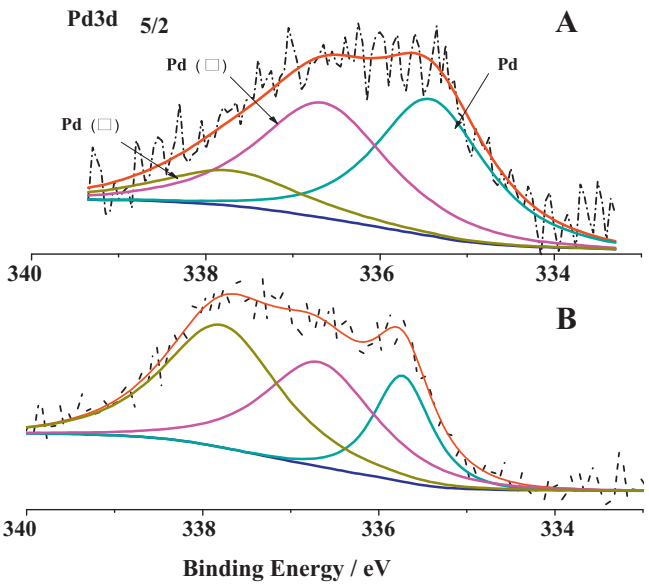

Fig. 4. XPS spectra of Pd 3d in the Pd/C-citrate catalyst (A) and the Pd-PMo_{12}/C catalyst (B).

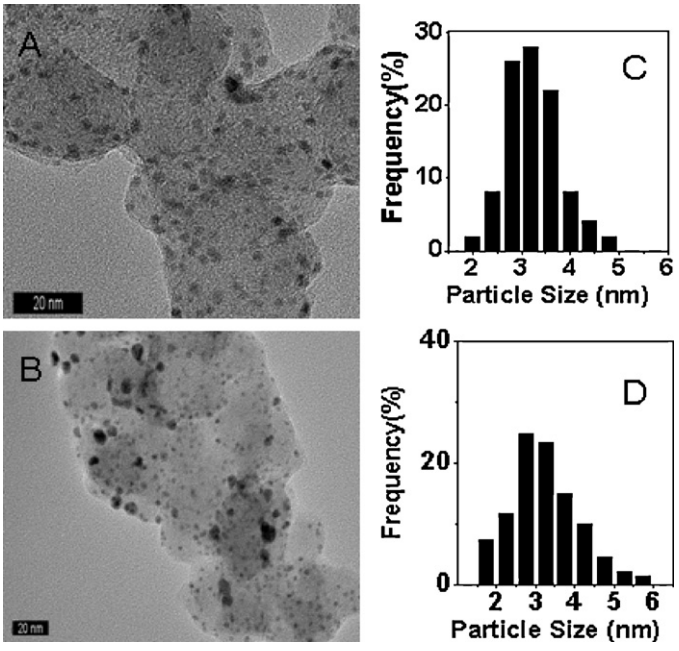

Fig. 3. TEM images and corresponding particle size distribution histograms of the Pd-PMo_{12}/C catalyst (A, C) and the Pd/C-citrate catalyst (B, D).

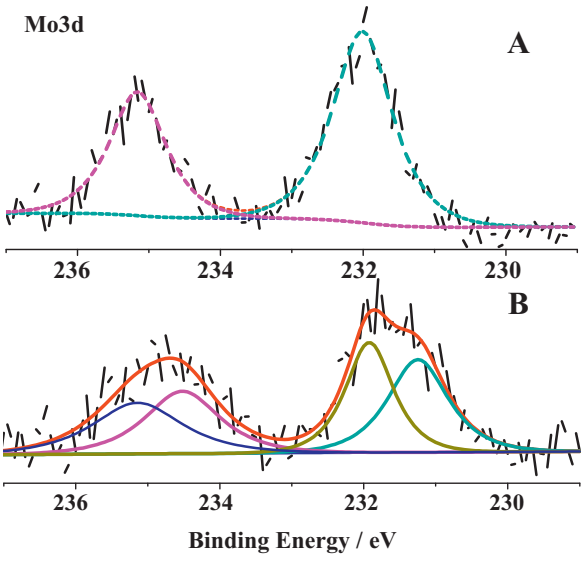

Fig. 5. XPS spectra of Mo 3d in PMo_{12}/C (A) and the Pd-PMo_{12}/C catalyst (B).

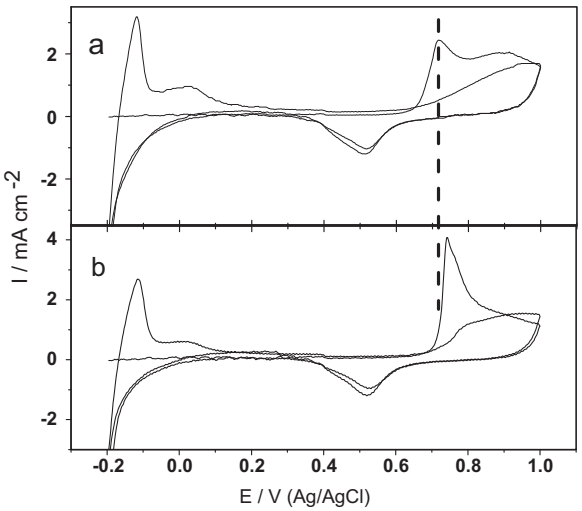

Fig. 6. CO-stripping voltammograms of the Pd-PMo_{12}/C catalyst (a) and the Pd/C-citrate catalyst (b) in 0.5 M H_2SO_4 solution with scan rate of 50 mV s^{-1}. The currents were normalized to the electrode area.

3.2. Electrochemical performance analysis

To evaluate the resistance to CO_{ads} poisoning, the CO_{ads} stripping curves of the two Pd catalysts were compared in Fig. 6. The peak potential of CO_{ads} oxidation for the Pd-PMo_{12}/C catalyst was 0.717 V, which is negatively shifted by 24 mV compared with the Pd/C-citrate catalyst at 0.741 V. This result indicated that the Pd-PMo_{12}/C catalyst has a much higher tolerance toward CO_{ads} poisoning than the Pd/C-citrate catalyst.

Fig. 7 shows the cyclic voltammograms (CVs) used to evaluate the electrocatalytic activities of the Pd-PMo_{12}/C and Pd/C-citrate catalysts for the FAEO. The two catalysts both showed a main peak at ca. 0.2–0.3 V, which was mainly attributed to the FAEO via the direct pathway, and a small shoulder peak near 0.5 V related to the

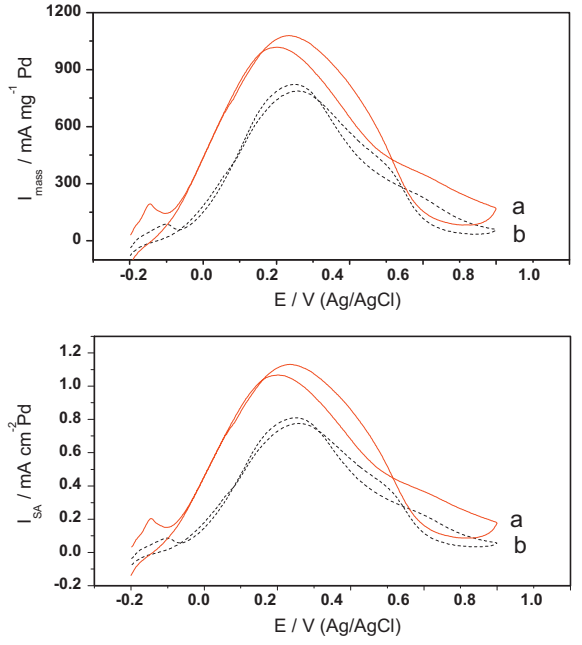

Fig. 7. Cyclic voltammograms of formic acid oxidation on the Pd-PMo_{12}/C catalyst (a) and the Pd/C-citrate catalyst (b) in 0.5 M H_2SO_4 + 0.5 M HCOOH solution with a scan rate of 20 mV s^{-1}. The currents were normalized to the mass of Pd (top) and the electrochemical surface areas of these catalysts (bottom).

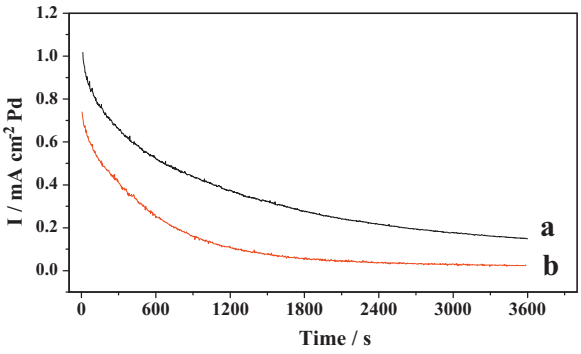

Fig. 8. Chronoamperometry of formic acid oxidation on the Pd-PMo_{12}/C catalyst (a) and the Pd/C-citrate catalyst (b) in 0.5 M H_2SO_4 + 0.5 M HCOOH solution potential, controlled at 0.2 V vs. Ag/AgCl.

oxidation of adsorbed CO-like species [8,26]. In the low potential region (below 0.3 V), a more useful potential region for DFAFCs, the Pd-PMo_{12}/C catalyst consistently displayed a much higher current density than the Pd/C-citrate catalyst. Specifically, the current density at 0.2 V for the Pd-PMo_{12}/C catalyst was 1017 mA mg^{-1} Pd which was 1.3-fold higher than that for the Pd/C-citrate catalyst (786 mA mg^{-1} Pd). In addition, the onset and peak potentials for the Pd-PMo_{12}/C catalyst were negatively shifted by 100 and 55 mV compared with the Pd/C-citrate catalyst. To compare the intrinsic activity of the catalysts, the current was normalized to the ESA of the catalysts, as shown in Fig. 7b. Clearly, an enhanced activity for the Pd-PMo_{12}/C catalyst was achieved relative to the Pd/C-citrate catalyst.

Fig. 8 shows the chronoamperometric curves at 0.2 V, which reflect the activity and the stability of catalysts. Consistent with the results of the CVs, the Pd-PMo_{12}/C catalyst possessed a much higher initial current density than the Pd/C-citrate catalyst. Considering the difference in the initial current of the catalysts, the current at 3600 s was normalized to the initial current to compare their stability. The calculated results were approximately 15% and 4% for the Pd-PMo_{12}/C and Pd/C-citrate catalysts, respectively. Given that the 'stability' could be defined as the decay rate of the catalyst, the chronoamperometric results demonstrated that the Pd-PMo_{12}/C catalyst had better stability during the FAEO compared to the Pd-PMo_{12}/C catalyst. It should be noted that the stability/decay rates of the catalyst was determined jointly by irreversible and reversible loss. The smaller particle size with a larger surface energy facilitated the growth and agglomeration of NPs, and led to a faster loss of electrochemical surface area. However, in light of the very small particle size differences between the Pd-PMo_{12}/C and Pd/C-citrate catalysts (3.2 nm vs. 3.5 nm), the difference in particle size was not the dominant factor in determining the decay rate of the studied Pd catalysts. In contrast, the poisoning effect played a more important role in determining the stability of the presented Pd catalysts. Indeed, the Pd-PMo_{12}/C catalyst with greater tolerance to CO-like poisoning species displayed a slower decay rate (85% loss per hour) than the Pd/C-citrate catalyst (96% loss per hour). In combination with the CVs data, this result substantially supported the finding that the Pd-PMo_{12}/C catalyst had an enhanced activity and stability for the FAEO. This result could be attributed to the following reasons. First, from previous reports, the metal–support interaction played a key role in determining the catalytic performances. This interaction modified the electronic and catalytic properties of metal NPs and led to the activation of both the dispersed metal and the support matrix for the electrode processes. The positive shift in BE for the Pd-PMo_{12}/C catalyst indicated a changed electronic structure and density of the state of Pd NPs. Zhou et al. [24] observed that the Pd NPs with higher BEs displayed an increased

activity for the FAEO. They attributed this observation to a decreased adsorption energy of the formate intermediate, which intrinsically enhances the rate of the FAEO via the direct pathway. Here, the higher BE for the Pd-PMo_{12}/C catalyst suggested an accelerated kinetic rate of the FAEO. This is in agreement with the data for the Pd-PMo_{12}/C catalyst, which had a higher current of 0.2 V, as compared with the Pd/C-citrate catalyst. Second, recent progress showed that the FAEO on the Pd surface gradually produced CO-like poisoning species which caused the deactivation of the Pd catalyst [8,27]. These species can only be oxidatively removed by a similar bifunctional mechanism (Pd—CO + Pd—OH → Pd + CO_2 + H^+ + e^-), in which oxygen-containing species on a neighboring surface site are necessary for the removal of CO_{ads} species [26,28]. The intrinsic presence or introduction of Pd oxides/hydrous oxides during the FAEO should promote the removal of the poisoning species, thereby leading to a better electrocatalytic property [4]. A richer Pd oxide/hydrous oxide species mix for the Pd-PMo_{12}/C catalyst may facilitate the oxidation of the CO-like intermediate by providing more available oxygen-containing species at lower potentials than the Pd/C-citrate catalyst. The CO_{ads} stripping tests demonstrated that the facile removal of CO-like intermediates adsorbed on the surface of the Pd-PMo_{12}/C catalyst promoted the activity and minimized performance degradation of the Pd-PMo_{12}/C catalyst. Lastly, according to previous reports, HPA anions showed the ability to facilitate the electrooxidation of intermediate species such as CO_{ads} or the CO-like species during methanol electroxidation [15,19,29,30]. Therefore, the redox property of PMo_{12} anions should have a positive effect on the removal of CO_{ads} oxidation for the Pd-PMo_{12}/C catalyst. The high protonic conductivity of PMo_{12} here facilitates the proton migration by the hydrogen spillover effect and thus accelerates the dehydrogenation of the FAEO on the Pd surface [15].

4. Conclusion

In this study, the Pd-PMo_{12}/C catalyst was prepared by introducing PMo_{12} using an impregnation reduction method. The as-prepared Pd NPs showed an average particle size of 3.2 nm and were uniformly dispersed on the carbon surface. In this study, PMo_{12} not only offered a large number of uniformly distributed active sites for anchoring Pd NPs but also protected Pd NPs form agglomeration by electrostatic repulsion effects. This synthesis method may also be useful in preparing other metal/carbon nanomaterials. More importantly, the Pd-PMo_{12}/C catalyst exhibited an enhanced activity and stability and a better CO_{ads} tolerance than the Pd/C-citrate catalyst. The enhanced electrocatalytic performance of the Pd-PMo_{12}/C catalyst for the FAEO was correlated with its metal–support interaction, richer hydrous PdO content and the inherent properties of PMo_{12}. The present structure-activity analysis may provide valuable features for the design and preparation of reactive and durable Pd-based nanocatalysts.

Acknowledgements

This work was supported by the National Natural Science Foundation of China (Nos. 20876153, 20703043, 21073180, 21011130027 and 20933004), the National High Technology Research and Development Program of China (863 Program, Nos. 2007AA05Z159 and 2007AA05Z143), the National Basic Research Program of China (973 Program, 2011CB935702), the Knowledge Innovation Project of CAS (KGCXZ-Y10-344) and the Science & Technology Research Programs of Jilin Province (Nos. 20102204 and 20100420).

References

[1] C. Rice, S. Ha, R.I. Masel, P. Waszczuk, A. Wieckowski, T. Barnard, J. Power Sources 111 (2002) 83–89.
[2] Z.H. Zhang, Y.J. Huang, J.J. Ge, C.P. Liu, T.H. Lu, W. Xing, Electrochem. Commun. 10 (2008) 1113–1116.
[3] C. Rice, S. Ha, R.I. Masel, A. Wieckowski, J. Power Sources 115 (2003) 229–235.
[4] M. Ren, Y. Kang, W. He, Z. Zou, X. Xue, D.L. Akins, H. Yang, S. Feng, Appl. Catal. B: Environ. 104 (2011) 49–53.
[5] X.W. Yu, P.G. Pickup, J. Power Sources 182 (2008) 124–132.
[6] X. Zhao, Y. Hu, L. Liang, C. Liu, J. Liao, W. Xing, Int. J. Hydrogen Energy 37 (2012) 51–58.
[7] J.L. Haan, K.M. Stafford, R.I. Masel, J. Phys. Chem. C 114 (2010) 11665–11672.
[8] X.W. Yu, P.G. Pickup, Electrochem. Commun. 11 (2009) 2012–2014.
[9] X.W. Yu, P.G. Pickup, Electrochem. Commun. 12 (2010) 800–803.
[10] W.J. Zhou, J.Y. Lee, Electrochem. Commun. 9 (2007) 1725–1729.
[11] L. Feng, X. Sun, C. Liu, W. Xing, Chem. Commun. 48 (2012) 419–421.
[12] Y.Y. Shao, J. Liu, Y. Wang, Y.H. Lin, J. Mater. Chem. 19 (2009) 46–59.
[13] X.W. Yu, S.Y. Ye, J. Power Sources 172 (2007) 133–144.
[14] X. Yu, S. Ye, J. Power Sources 172 (2007) 133–144.
[15] Z.P. Guo, D.M. Han, D. Wexler, R. Zeng, H.K. Liu, Electrochim. Acta 53 (2008) 6410–6416.
[16] Y.Y. Shao, G.P. Yin, J. Zhang, Y.Z. Gao, Electrochim. Acta 51 (2006) 5853–5857.
[17] D.W. Pan, J.H. Chen, W.Y. Tao, L.H. Nie, S.Z. Yao, Langmuir 22 (2006) 5872–5876.
[18] M. Sadakane, E. Steckhan, Chem. Rev. 98 (1998) 219–238.
[19] M.H. Seo, S.M. Choi, H.J. Kim, J.H. Kim, B.K. Cho, W.B. Kim, J. Power Sources 179 (2008) 81–86.
[20] R. Wlodarczyk, M. Chojak, K. Miecnikowski, A. Kolary, P.J. Kulesza, R. Marassi, J. Power Sources 159 (2006) 802–809.
[21] Z.M. Cui, W. Xing, C.P. Liu, D. Tian, H. Zhang, J. Power Sources 195 (2010) 1619–1623.
[22] S. Ozkar, R.G. Finke, J. Am. Chem. Soc. 124 (2002) 5796–5810.
[23] Z. Cui, P.J. Kulesza, C.M. Li, W. Xing, S.P. Jiang, Int. J. Hydrogen Energy 36 (2011) 8508–8517.
[24] W.P. Zhou, A. Lewera, R. Larsen, R.I. Masel, P.S. Bagus, A. Wieckowski, J. Phys. Chem. B 110 (2006) 13393–13398.
[25] L.A. Ma, X.A. Zhao, F.Z. Si, C.P. Liu, J.H. Liao, L.A. Liang, W. Xing, Electrochim. Acta 55 (2010) 9105–9112.
[26] W. Zhou, J.Y. Lee, J. Phys. Chem. C 112 (2008) 3789–3793.
[27] H. Miyake, T. Okada, G. Samjeske, M. Osawa, PCCP 10 (2008) 3662–3669.
[28] X. Zhao, M. Yin, L. Ma, L. Liang, C. Liu, J. Liao, T. Lu, W. Xing, Energy Environ. Sci. 4 (2011) 2736–2753.
[29] W.B. Kim, T. Voitl, G.J. Rodriguez-Rivera, J.A. Dumesic, Science 305 (2004) 1280–1283.
[30] L. Feng, X. Zhao, J. Yang, W. Xing, C. Liu, Catal. Commun. 14 (2011) 10–14.